university of groningen

University Medical Center Groningen

University of Groningen

Charge transport and trap states in lead sulfide quantum dot field-effect transistors

Nugraha, Mohamad Insan

IMPORTANT NOTE: You are advised to consult the publisher's version (publisher's PDF) if you wish to cite from it. Please check the document version below.

Document Version
Publisher's PDF, also known as Version of record

Publication date:
2017

Link to publication in University of Groningen/UMCG research database

Citation for published version (APA):
Nugraha, M. I. (2017). *Charge transport and trap states in lead sulfide quantum dot field-effect transistors*. [Thesis fully internal (DIV), University of Groningen]. University of Groningen.

Copyright
Other than for strictly personal use, it is not permitted to download or to forward/distribute the text or part of it without the consent of the author(s) and/or copyright holder(s), unless the work is under an open content license (like Creative Commons).

The publication may also be distributed here under the terms of Article 25fa of the Dutch Copyright Act, indicated by the “Taverne” license. More information can be found on the University of Groningen website: https://www.rug.nl/library/open-access/self-archiving-pure/taverne-amendment.

Take-down policy
If you believe that this document breaches copyright please contact us providing details, and we will remove access to the work immediately and investigate your claim.

Downloaded from the University of Groningen/UMCG research database (Pure): http://www.rug.nl/research/portal. For technical reasons the number of authors shown on this cover page is limited to 10 maximum.

Download date: 29-04-2025

Chapter 1

Introduction

This chapter gives an overview of the physical properties (including charge transport and optical properties) of semiconducting colloidal quantum dots based on lead sulfide (PbS), and research progresses on the use of these colloidal quantum dots for the fabrication of field-effect transistors (FETs). Some potential methods for improving charge carrier mobility in PbS FETs will be discussed. In the final section, the experimental techniques used and the outline of this thesis will be provided.

1.1 Colloidal Quantum Dots

Semiconductor colloidal quantum dots (QDs), often also called nanocrystals (NCs), are a class of solution processable crystalline materials with size ranging from 1 to 20 nm.[1] Due to their tiny dimensions, QDs consist of only few hundreds to thousands atoms. With this finite number of atoms, the properties of QDs resemble those of atoms showing quantization of their energy levels, for which reason they are also often called artificial atoms.[2–5] Indeed, when the size of QDs is smaller than their exciton Bohr radius, strong quantum confinement of charge carrier wave-function, which leads to size-dependent electronic and optical properties, is displayed.[6–8] This size-tunable phenomenon due to the quantum confinement is commonly called as quantum size effect.

Among many types of QDs which have been introduced in the last years, lead sulfide (PbS) QDs are one of the most interesting particularly because they have large exciton Bohr radius (~20 nm) and at the same time possess straightforward and well-established synthetic methods which give rise to high quality materials.[9–12] As a result of the large exciton Bohr radius, strong quantum confinement can be effectively achieved to control the band gap of the PbS QDs from 0.4 to 2 eV by tuning their size from bulk to 2 nm.[13,14] Because of this size-tunable band gap, PbS QDs have been used as promising semiconducting building blocks for highly efficient optoelectronic devices such as solar cells,[15–25] photodetectors,[26–28] and light-emitting devices.[8,29] More recently, the solution processability of these QDs has also attracted great attention for the fabrication of field-effect transistors.[30–42]

PbS QDs are synthesized using the so-called hot injection process by rapidly injecting organometallic precursors into a hot solvent containing organic surfactants.[10,12] The organic surfactants consist of long-chain hydrocarbon compounds such as oleic acid,[43,44] n-octadecylphosphonic acid,[35] trioctylphosphine oxide (TOPO),[45] and hexadecylamine.[46,47] When the organometallic precursors are rapidly injected into the mixture of the hot solvent and the organic surfactants, a decrease of temperature initiates the nucleation of the compounds, which is followed by particle growth after reheating the final mixture. The long-chain hydrocarbon surfactants, organic ligands, play an important role in determining the kinetics of nucleation and growth in the solution.[46] The key synthesis parameters need to be balanced in order to obtain monodisperse colloidal QDs with controllable size. The monodisperse QDs which should possess identical shape, structure, size, and surface chemical properties result in samples with narrow emission bandwidth and high luminescence efficiencies.[12] The high resolution transmission electron microscopy (HRTEM) images of monodisperse PbS QDs (with diameter of 3.6 nm) are shown in Figure 1.1 (a) and (b).

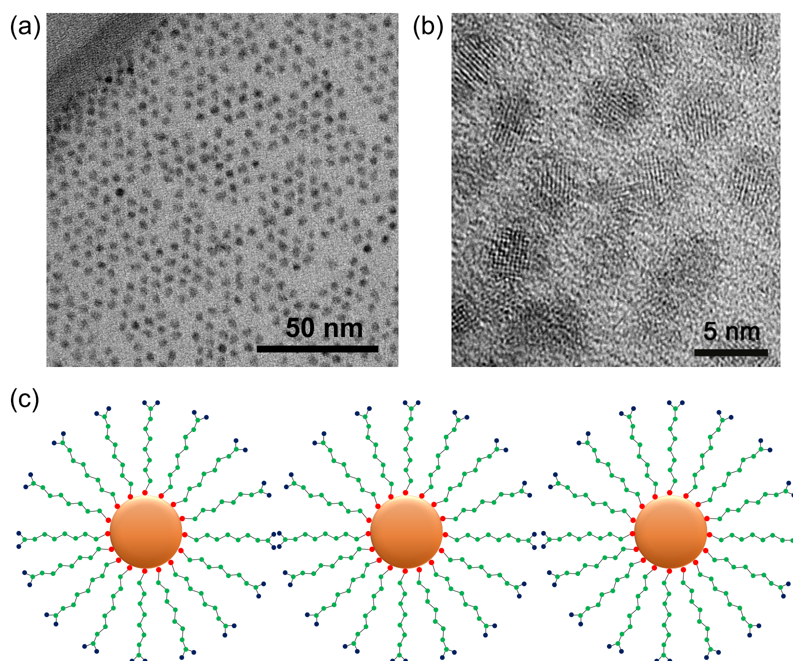

Figure 1.1 High resolution transmission electron microscopy (HRTEM) images of PbS QDs at (a) low and (b) high magnification. (c) Schematic of PbS QDs with long organic ligands on their surfaces.

The long ligands are also fundamental as stabilizers for the colloidal dispersion by capping the QD surfaces, and preventing particle aggregation. The ligands generally used provide good QD dispersibility in most organic solvents.[46] These allow QD thin films to be deposited using low cost and low temperature solution processed methods such as spin-coating,[27] blade-coating,[28] dip-coating,[40], and roll-to-roll processes.[40] Figure 1.1 (c) presents the schematic of PbS QDs with long ligands on their surfaces. When PbS colloidal QDs are assembled onto thin film solids, the ligands behave as tunneling barriers, which maintain the quantum confinement of the individual QDs.

1.2 Electronic structures of QDs

1.2.1 Quantum confinement

Due to complete quantum confinement of charge carrier wave function, the electronic structures of QDs have unique characteristics with respect to their parent bulk materials and other material structures such as quantum wells and quantum wires. In bulk materials, charge carriers are fully delocalized. The

carriers move through the energy bands formed due to the overlap of wave functions between neighboring atoms. According to the nearly-free electron model, charge carriers in bulk materials have almost continuous energy spectrum (E) (vide infra) and the density of states in this system is proportional to $E^{1/2}$.[48] By reducing the material dimension, the bulk materials turn to quantum wells (two-dimensional structure – confined in 1 direction) and quantum wire structures (one-dimensional structure – confined in 2 directions), or to a quantum dot (zero-dimensional structure – confined in 3 directions) as demonstrated in Figure 1.2. As a consequence of the quantum confinement, the density of states in quantum wells and quantum wires displays unique profiles showing increment of the density of electronic states only at certain energy.[49]

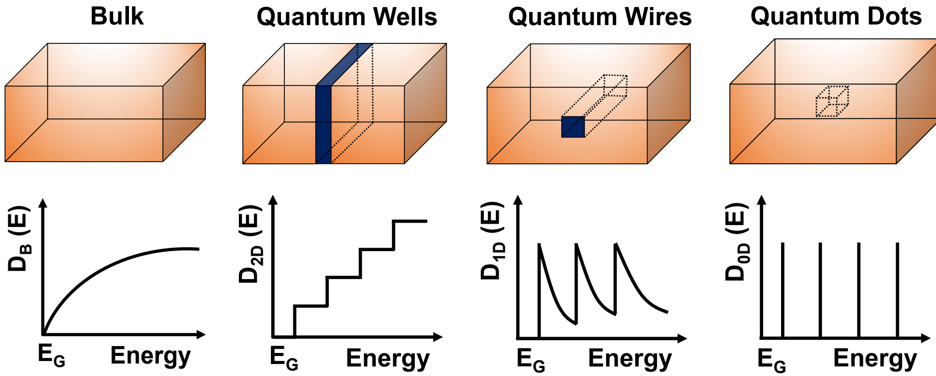

Figure 1.2 Quantum confinement and density of states in materials with different dimensionality.

In QDs, charge carriers are confined in all directions of the materials as demonstrated in Figure 1.2. With the quantum confinement, the density of states in QDs appears as the delta Dirac function, which again displays the characteristics of energy quantization. As mentioned, the quantum confinement in QDs becomes active when the size or radius of the particles is smaller than the exciton Bohr radius (R_B),[50]

$$R_B = \frac{\hbar^2 \varepsilon}{e^2 \mu} \tag{1.1}$$

where ε, $\hbar$, μ, and e are dielectric constant, reduced *Planck* constant, reduced mass of holes and electrons, and elementary charge constant, respectively. In PbS, the exciton Bohr radius can be as large as 20 nm which effectively allows strong quantum confinement even in relatively large sized particles with respect to other materials such as CdSe (R_B=5.6 nm),[51] CdS (R_B=2.8 nm),[52,53] and ZnO (R_B=2.87 nm).[54]

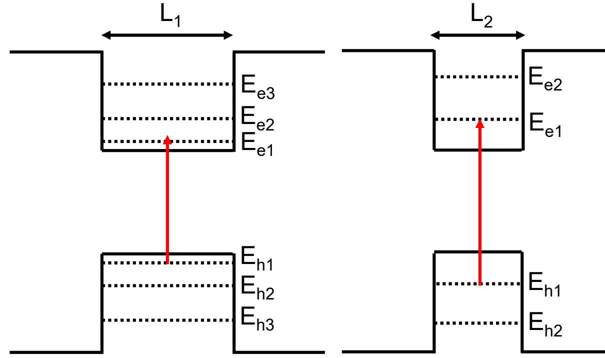

Figure 1.3 Quantum confinement and size effect in QDs. The dash lines show discrete energy levels in QDs. The band gap (red lines) increases with decreasing the QD size.

Many studies have been performed to understand the electronic structures of QDs.[55,56] A simple approach to study their electronic structures is based on the strongly confined particle model in a square potential well as demonstrated in Figure 1.3. The potential barrier is produced by the surface of QDs and the ligands on the QD surface. By applying the Schrodinger equation, the energy levels (E_n) of carriers in QDs are quantized as:

$$E_n = \frac{\hbar^2 \pi^2}{2m^*}\left(\frac{n_x^{\ 2}}{L_x^{\ 2}} + \frac{n_y^{\ 2}}{L_y^{\ 2}} + \frac{n_z^{\ 2}}{L_z^{\ 2}}\right) \quad (1.2)$$

where m^* is the effective mass of holes and electrons in QDs. L_x, L_y, and L_z are the size of QDs in x, y, and z direction respectively. The three integer quantum numbers (n_x, n_y, and n_z) indicate the quantization of energy in the directions. The first transition energy, thus the band gap, can be estimated from the difference of the ground state energy of electrons and holes (E_G=E_{e1}-E_{h1}) as demonstrated in Figure 1.3. This ground state energy is inversely proportional to the QD size as stated in equation (1.2). As a consequence, the band gap (E_G) of QDs increases with decreasing the particle size. The size-tunable band gap of QDs is shown in Figure 1.3.

Another approximation for the electronic structures of QDs is using a spherical potential model.[49,56] By solving the Schrodinger equation in spherical coordinates, the energy levels of charge carriers in QDs with radius R can be written as:[49]

$$E_{n,l} = \frac{\hbar^2 \pi^2}{2m^* R^2} \chi_{n,l}^{\ 2} \quad (1.3)$$

where $\chi_{n,l}$ is the nth zero of the lth-order spherical Bessel function. The schematic of energy levels in spherical QDs is shown in Figure 1.4.

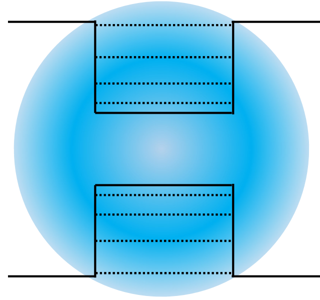

Figure 1.4 Energy levels of spherical QDs with radius R.

A more comprehensive analysis involving the effective mass model shows that the energy of the first excited electronic states (band gap energy) in QDs with radius R can be stated as,[57,58]

$$E_G = E_G^{bulk} + \frac{\hbar^2 \pi^2}{2R^2}\left(\frac{1}{m_e^*} + \frac{1}{m_h^*}\right) - \frac{1.8e^2}{4\pi\varepsilon\varepsilon_o R} \qquad (1.4)$$

where E_G^{bulk} and ε_o are the bulk band gap energy and vacuum permittivity constant, respectively. The third term in equation (1.4) corresponds to the Coulomb interaction between holes and electrons in the QDs. In line with the square-shaped QDs, the band gap energy of spherical QDs increases with decreasing the radius of the QDs.

1.2.2 Role of capping ligands

The ligands have the double role of stabilizing the QD colloidal solution and to guarantee the quantum confinement over long time. For this reason they are chosen to be well insulating. This also means that when the QDs are organized in a film, the ligands suppress charge transport within the QD film. To improve the film conductivity, the long ligands need to be exchanged with shorter ones. This ligand exchange can be done either in solution or in solid state.[59–61] Several short ligands have been shown to enable charge transport while still maintaining quantum confinement within the QD solids.[62,63] As this statement can appear peculiar, it needs to be clarified in the sense that the short ligands allow carriers to tunnel between QDs while the QD films still show quantum confinement in terms of their band gap and optical properties.

The short ligands can be organic (e.g. 3-mercaptopropionic acids/3MPA,[64] benzenethiols/BT,[65] benzene-dithiols/BDT,[66] 1,2-ethanedithiols/EDT,[67] 1,2-ethylenediamine/EDA,[68] thiocyanates/SCN^-,[33] etc) or inorganic molecules or single atoms (e.q. metal chalcogenides,[46,47] halometallates,[62] halide anions,[60] etc). The chemical structures of some of the most common ligands are shown in Figure 1.5 (a). As a result of the ligand exchange, the exchange coupling energy

(β), related to the tunneling rate of charge carriers between QDs, increases. The exchange coupling energy can be written as:[1]

$$\beta = \hbar \exp\left[-2\left(2m^{*}E_{b}/\hbar^{2}\right)^{1/2} d \right] \quad (1.5)$$

where E_b and d are the potential barrier height and the inter-QD distance, respectively. From equation (1.5), it is obvious that the tunneling rate of charge carriers increases with decreasing the inter-QD distance. In agreement with equation (1.5), Law et al. reported that the charge carrier mobility in lead chalcogenide QD systems increases exponentially with decreasing ligand length, thus the inter-QD distance.[7]

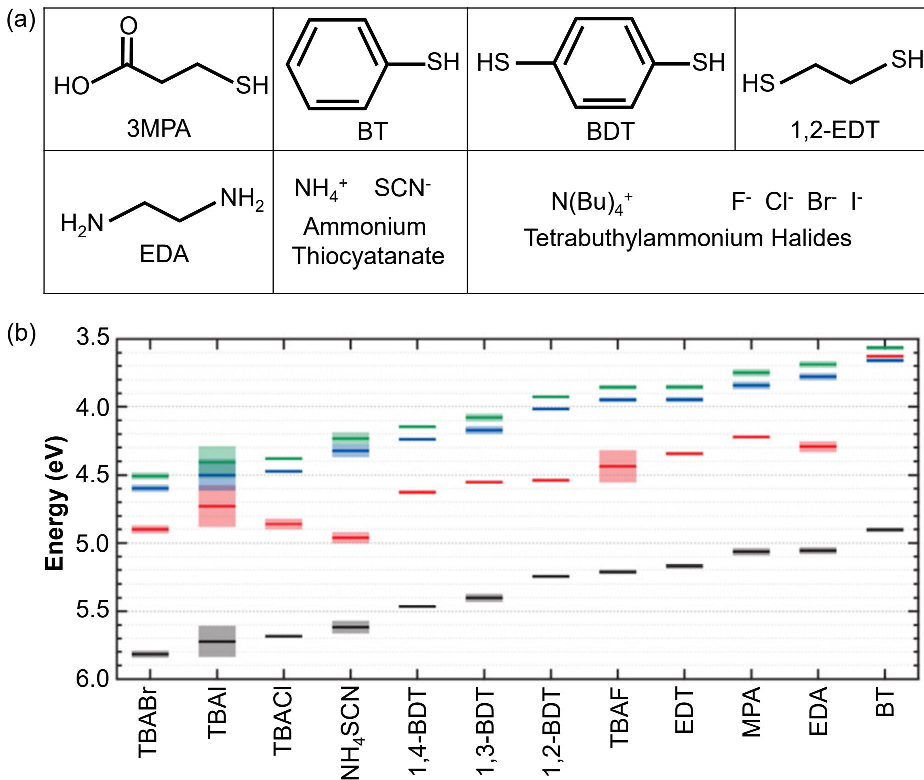

Figure 1.5 (a) Chemical structures of ligands and (b) energy levels of PbS QDs with different ligands. The black and red lines correspond to the valence bands and Fermi levels of the materials, respectively. The green and blue lines are the optical and transport conduction bands of the materials, respectively. Tetrabuthylammonium halide ligands (TBAX, X=Br, I, Cl) produce deeper conduction bands than those with thiol-based ligands. The data of the energy levels are extracted from literature.[69]

The short capping ligands on the QD surfaces also modify the electronic structures of PbS QDs. As referred to Figure 1.5 (a), the short ligands may change dielectric environment between neighboring QDs. The ligands with their different dipole moments can influence the energy alignment inside QDs. As a result, the electronic structures of QDs including the vacuum energy, Fermi level, valence band, and conduction band can be affected. Brown et al. reported energy level modification in PbS QD films using various ligands.[69] The same authors reported a comprehensive energy level schematic of PbS QD films with different capping ligands that is reproduced in Figure 1.5 (b). Although capped with similar bidentate thiols (BT and 1,4-BDT), a significant shift of the conduction and valence bands up to 0.7 eV is observed. With halide-based ligands, the conduction bands of the PbS QD films can be as deep as -4.5 eV (TBABr). With these significant shifts, the use of particular capping ligands can determine the performance of electronic devices based on PbS QDs by controlling the charge extraction between injection/extraction contacts and the semiconducting films.

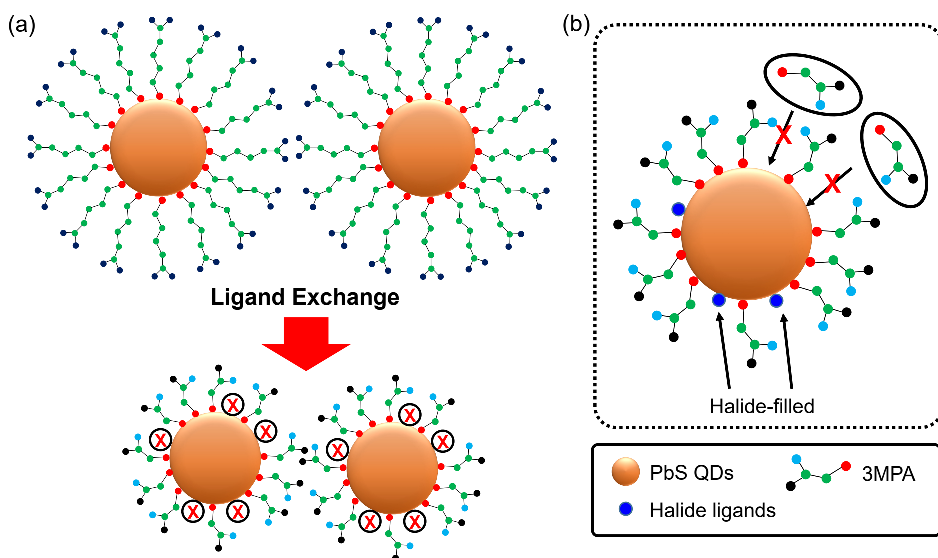

Figure 1.6 (a) Schematic of ligand exchange. Due to incomplete ligand exchange reaction, some dangling bonds on the QD surfaces are formed. (b) Schematic of PbS QDs passivated with organic ligands (3MPA) and hybrid organic/inorganic (3MPA/halide) ligands. Due to their large size, some 3MPA molecules are not able to penetrate into some inter-cation trenches. The schematic is adapted from reference.[16]

The high surface area to volume ratio of QDs, typical of nano-objects, makes them more prone to develop a high number of traps on the QD surfaces. These carrier traps are extremely important as they limit the performance of the

electronic devices based on QDs. The carrier traps may originate from structural aperiodicity and off-stoichiometry composition of the QDs.[70] The ligands take also an important role in providing surface passivation against carrier traps. Nevertheless, after the exchange of the long ligands to shorter ones, some surface dangling bonds may also be formed because of an incomplete ligand exchange reaction. These dangling bonds can indeed act as additional carrier traps on the QD surfaces as schematically shown in Figure 1.6 (a). Ip et al., found that steric interactions prevent some short organic ligands such as 3MPA from penetrating the inter-cation trenches on the QD surfaces as displayed in Figure 1.6 (b).[16] As a result, some un-passivated QD surfaces remain which act as additional traps.

In comparison to organic ligands such as 3MPA and other thiol-based ligands, halide ligands have been reported to provide an effective passivation against carrier traps that results in high performance FETs and highly efficient solar cells based on PbS colloidal QDs.[15,63] However, recently Balazs et al., have also underlined the importance of counterions (ammonium, methylammonium, tetrabuthylammonium in iodide salts) in the ligand-exchange mechanism.[63] Since they have specific reactivity and acidity, the types of counterions can determine the effectiveness of the ligand exchange reaction, thus the removal of native long organic ligands. With the treatment of the first two ligands, efficient charge transport in the PbS films is revealed, as indicated from the high film conductivity. Particularly, the films treated with methylammonium iodide enable good performing transistors with electron mobility of 0.05 $cm^2V^{-1}s^{-1}$ and on/off ratio of 10^6. Meanwhile, among those ligands, the films treated with tetrabuthylammonium iodide show poor conductivity. The lower reactivity of tetrabuthylammonium iodide than that of others results in incomplete removal of the native long insulating ligands on the QD surfaces, suppressing the charge transport between neighboring particles.

1.3 Optical properties of PbS QDs

Similar to their unique electronic structures, the optical properties of QDs are also size-dependent as a result of the quantum confinement effect. In addition, when colloidal QDs are assembled onto thin film solids, the distance between QDs determines the electronic coupling between neighboring QDs. The change of the electronic coupling between QDs also influences their optical properties. In this section, the effect of QD size and inter-QD distance on the optical properties of PbS QDs is reviewed.

1.3.1 Effect of QD size

QDs are characterized by strong excitonic interactions that are displayed from the strong (excitonic) peak in the lower energy region of the absorbtion spectrum. Figure 1.7 shows the absorbance spectrum of PbS QDs with different sizes. It is obvious that the excitonic peaks are red-shifted with increasing the QD size, also indicating the decrease of the band gap. In 3.7 nm PbS QDs, the excitonic wavelength is about 1100 nm, which corresponds to the band gap of 1.13 eV. This band gap as explained earlier is larger than that of bulk PbS (E_G=0.41 eV). By increasing the QD size to 6.5 nm, the excitonic wavelength shifts to 1660 nm. Meanwhile, when the QD size is reduced to 2 nm, a blue-shifted excitonic wavelength results in the band gap of 2 eV.[14] With the size-tunable optimal band gap properties, PbS QDs allow optimal utilization of the solar spectrum particularly in the near-infrared region which is beneficial to realize highly efficient solar cells.

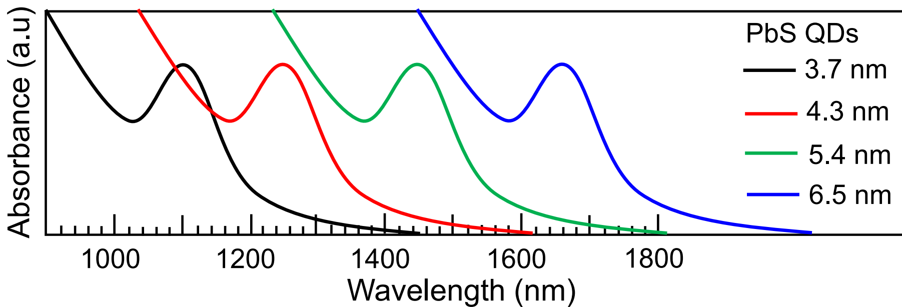

Figure 1.7 Absorbance spectrum of PbS QDs of different sizes. The spectrum are modified from reference.[14]

1.3.2 Effect of inter-QD distance

In QD films, the inter-QD distance determines the electronic coupling between QDs. When they are at a large distance, the electronic coupling between QDs is very small and charge transport does not occur. In this regime, the QD arrays have approximately identical electronic and optical properties as individual QDs. As the inter-QD distance is reduced, the electronic coupling between QDs becomes important. Consequently, the carrier wave function can extend over the films, which influences the electronic structures and the optical properties of the QD films. Several groups have reported that the excitonic peaks of CdSe and InP QD films in the absorbance spectrum shift to the red by reducing the inter-QD distance.[71,72] Similarly, a red-shifted profile of the absorbance spectrum of PbS

films is also observed by reducing the inter-QD distance from the use of long oleic-acid (OA) and short EDT ligands as presented in Figure 1.8.

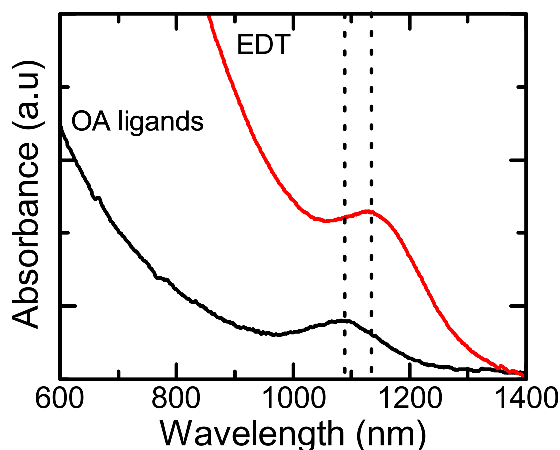

Figure 1.8 Absorbance spectra of PbS QD films with OA and EDT ligands.

The decrease of the inter-QD distance can also be achieved by annealing the QD films at higher temperature. However, the high annealing temperature may result in sintering of the QDs leading to the vanishing of quantum confinement within the QD films. Sintering the QD films is undesirable particularly for photovoltaics, where the loss of quantum confinement results in lower open circuit voltage and consequent reduction of the device performance.[73] Recently, the use of different types of atomic ligands puts also in evidence for the formation of necking, which is shown by the continuity of the PbS crystal lattice along a particular facet.[63] In PbS QDs, three main facets define their crystal structure, namely {100}, {110}, and {111}. The last two facets have more acidity than the {100} facets, and at the same time have higher surface energy than un-passivated {100} facets, which promote the removal of anionic ligand species from the {100} facets.[63] This anionic ligand species removal is then followed by the diffusion of Pb and S atoms along {100} facets, indicating the formation of necking along this direction. Consequently, the PbS films show reduced band gap and weaker excitonic signatures.

Recently, the application of external mechanical pressure has also been reported to influence the inter-QD distance.[13,74] The effect of pressure on the inter-QD distance is demonstrated by the red-shifted excitonic peaks in the absorbance spectrum of the PbS films with increasing the pressure. The red-shifted profiles indicate the decrease of the inter-QD distance, which is attributed to the bending of the capping ligands on the QD surfaces. As the transport of

charge carriers within the QD films is strongly influenced by the inter-QD distance, this effect can also be used to tune the charge transport properties in the QD films.

1.4 PbS QD field-effect transistors (FETs)

Understanding charge transport in PbS QD solids has recently become an important research interest in the QD community. One of effective tools for this investigation is the fabrication of field-effect transistors (FETs).[75–78] The fabrication and characterization of FETs are one of the most straightforward methods to obtain information on charge carrier mobility and to study transport mechanisms in semiconductors. This section is devoted to provide an overview about the basic operational principles of FETs as well as some research progress related to the methods to improve charge transport in PbS QD-FETs.

1.4.1 Basic operation of FETs

In their structure, FETs use three materials including metal, insulator, and semiconductor as main components. Figure 1.9 (a) shows the schematic of an FET with channel length L and width W. FETs have 3-terminal configuration namely gate, source, and drain electrodes. In general, the source electrode is connected to the ground whereas the gate and drain electrodes are connected to a voltage source. In FETs, the semiconductor and the gate electrode are separated by a thin layer of insulator. By applying a voltage to the gate electrode, charge carriers are accumulated at the semiconductor/insulator interface. These accumulated charge carriers form a conducting path where charge carriers can flow from the injecting electrode (source) to the collecting electrode (drain). The minimum gate voltage (V_g) that is required to form the conducting channel is defined as threshold voltage (V_{th}).

Depending on the semiconductor, FETs can show n- or p-type or ambipolar properties. In n-type FETs, when a positive gate voltage is applied, the Fermi level of the gate electrode is shifted down resulting in downward bending of the conduction band (CB) and valence band (VB) of the semiconductor. Consequently, electrons are accumulated at the semiconductor/insulator interface. Meanwhile, in p-type FETs, when a negative gate voltage is applied, the Fermi level of the gate electrode is shifted up. This condition results in upward bending of the CB and VB leading to hole accumulation at the semiconductor/insulator interface. In ambipolar FETs, both electrons and holes are accumulated at the semiconductor/insulator interface depending on the polarity of the gate voltage. Figure 1.9 (b)-(d) show the schematics of energy diagram in FETs with several gate bias conditions.

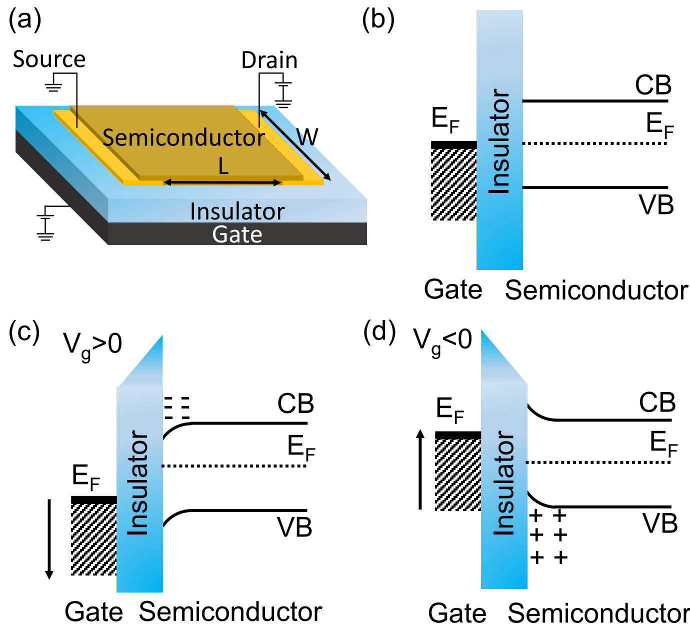

Figure 1.9 (a) Schematic of an FET device. Energy band diagram in an FET with (b) zero, (c) positive, and (d) negative gate voltages.

The electrical behavior of an FET is determined by measuring two types of I-V characteristics, namely the output and transfer characteristics. The output characteristics of FETs are obtained by measuring the source-drain current (I_{ds}) as a function of source-drain voltage (V_{ds}) at fixed V_g. The transfer characteristics are obtained by measuring the source-drain current (I_{ds}) while sweeping the V_g at a fixed V_{ds}. The transfer characteristics demonstrate the effectiveness of the gate voltage in modulating the electrical current in the devices and in switching the devices from the off to the on-state. When a $V_{ds} << (V_g - V_{th})$ is applied on the FETs, as mentioned already charge carriers are accumulated forming a conducting path with homogeneous carrier density as demonstrated in Figure 1.10 (a). The conducting path forms a channel connecting source and drain which allows the flow of electrical current. In this condition, the FETs behave like a resistor where the current increases linearly with increasing V_{ds}, which is referred to as the linear regime. The source-drain current in the linear regime is written as,

$$I_{ds} = \frac{\mu C_i W}{L}\left[\left(V_g - V_{th}\right)V_{ds} - \frac{V_{ds}^{\ 2}}{2}\right] \tag{1.6}$$

where μ and C_i are the charge carrier mobility in the devices and the capacitance of the gate insulator. It is important to note that the above equation assumes the

absence of contact resistances at the source and drain contacts, thus an Ohmic contact. In the presence of a Schottky barrier between the source/drain work function and CB/VB of the semiconductor, FETs show S-shaped output characteristics in the linear regime at low V_{DS}.

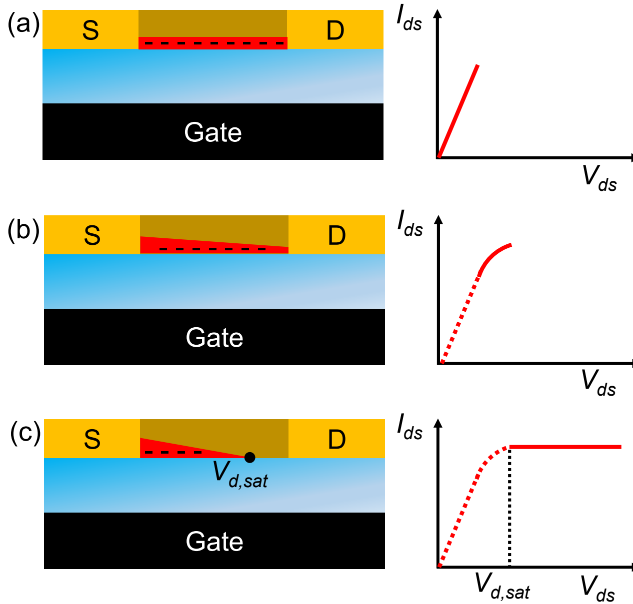

Figure 1.10 Schematic view of the basic working principles of FETs in (a) the linear, (b) parabolic, and (c) saturation regime, with corresponding I_{ds}-V_{ds} output characteristics.

As the V_{ds} increases, the voltage drop across the insulator near the drain decreases resulting in non-uniformity of the density of accumulated carriers as displayed in Figure 1.10 (b). As a consequence, the channel resistance of the devices increases, leading to a decrease of the slope of the output characteristics. At this point, the transistors operate in the parabolic regime. In this regime, I_{ds} will depend on the other parameters as expressed in equation (1.6). In the linear regime, the second term in the equation (1.6) is much smaller than the first part allowing neglecting the quadratic term, which preserves the linearity of the output characteristics. However, as the V_{ds} increases, the second part of the equation will become important, resulting in the parabolic shape of the output characteristics.

When the V_{ds} is further increased ($V_{ds} >> (V_g-V_{th})$), the accumulated charge carriers move toward the source electrode. At a given V_{ds}, the so-called $V_{d,sat}$, is reached, then the density of the accumulated carriers is zero at the drain electrode. In this condition, the charge carriers travel through the channel toward the drain electrode. At the point where the carrier density goes to zero, so-called pinch-off

point demonstrated as $V_{d,sat}$ in Figure 1.10 (c), the charge carriers are swept by the electric field between the pinch-off point and the drain electrode, and flowing through the space-charge region. In the ideal condition, the increase of the conductance is zero, thus the source-drain current is constant, since the electric current is only governed by the carrier diffusion through the space-charge region (between pinch-off point and the drain electrode). This condition is called saturation regime since the source-drain current saturates (constant) even though the V_{ds} increases as demonstrated in Figure 1.10 (c). In the saturation regime, the source-drain current can be expressed with the equation:

$$I_{ds} = \frac{\mu C_i W}{2L}\left(V_g - V_{th}\right)^2 \qquad (1.7)$$

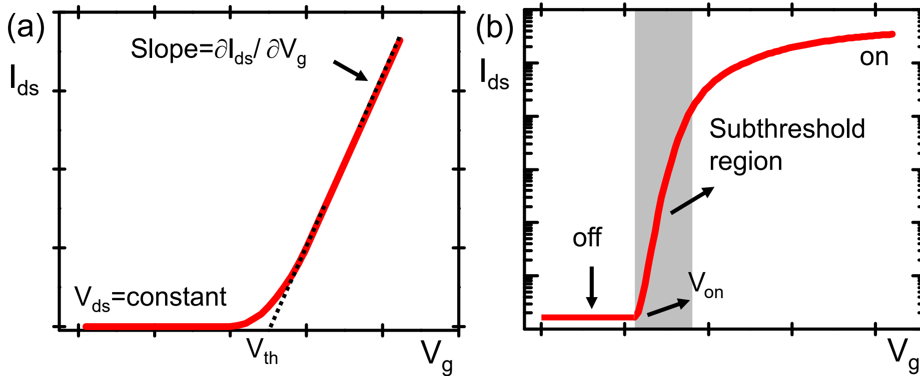

Figure 1.11 The I_{ds}-V_g transfer characteristics of FETs in (a) the linear and (b) semi-logarithmic scale.

The transfer characteristics are obtained by measuring the I_{ds} and sweeping V_g at a given V_{ds}. As previously mentioned, when a V_g is applied, the charge carriers are accumulated at the semiconductor/insulator interfaces forming a conducting path (channel) between the source and drain electrodes. When the V_g is lower than the threshold voltage (V_{th}), no current flows through the channel. As the V_g gradually increases beyond the V_{th}, the density of the accumulated charge carriers increases which results in the decrease of the channel resistance. Consequently, the I_{ds} increases with increasing the V_g. In the ideal condition, no current flows to the gate because the gate electrode is separated by an insulating layer. The typical I_{ds}-V_g transfer characteristics of FETs in the linear scale are shown in Figure 1.11 (a). By measuring the transfer characteristics, the charge carrier mobility in the linear regime (μ_{lin}) can be derived as,

$$\mu_{lin} = \frac{L}{WC_iV_{ds}}\frac{\partial I_{ds}}{\partial V_g} \qquad (1.8)$$

where $\partial I_{ds}/\partial V_g$ is the transconductance that can be calculated from the slope of the transfer characteristics of the devices. The mobility in the saturation regime (μ_{sat}) is derived from equation (1.7) and stated as,

$$\mu_{sat} = \frac{2L}{C_i W}\left(\frac{\partial I_{ds}^{1/2}}{\partial V_g}\right)^2 \qquad (1.9)$$

where $\partial I_{ds}^{1/2}/\partial V_g$ is calculated from the slope of the square root of I_{ds} versus V_g characteristics.

At this point, it is important to consider the I_{ds}-V_g transfer characteristics in the semi-logarithmic scale as displayed in Figure 1.11 (b). The V_g where the current starts increasing exponentially is defined as on-voltage (V_{on}). The V_{on} also provides information on the doping level in FETs. Moreover, Figure 1.11 (b) also shows the off- and on-state of the devices. The ratio of on-current and off-current is defined as the on/off ratio, which indicates the ability of the devices to be switched from the off- to on-state. Good performing FET devices are expected to have high on-off ratio, the precise figure of merit will mostly depend on the application.

The semi-logarithmic profile of the transfer curve also reveals another important regime in the FET devices.[79] The so-called subthreshold regime, displayed in Figure 1.11 (b), occurs when the applied gate voltage is below the threshold voltage of the devices. In this regime, the current is mainly governed by the diffusion process, which is independent of the drain voltage ($V_{ds} << k_B T/q$). The diffusion current is a consequence of the large gradient of the charge carrier concentration between the source and drain contact regions, and is thus dependent on the gate voltage,

$$I_{ds} \propto \exp\left(\frac{eV_g}{n^* k_B T}\right) \qquad (1.10)$$

where e, k_B, and T are charge constant, Boltzmann constant, and temperature, respectively. The ideality parameter (n^*) corresponds to the density of carrier traps in the devices, which originates from the semiconductor/insulator interface and the bulk of semiconductor.[79] The subthreshold swing (SS) and the ideality parameter are defined as,

$$SS = \frac{k_B T \ell n 10}{e} n^* \qquad (1.11)$$

$$n^* = 1 + \frac{C_{sc}}{C_i} \qquad (1.12)$$

where C_{sc} is the capacitance of semiconductor. The C_{sc} is related to the density of traps in the devices which influences the transfer characteristics of the devices in the subthreshold regime, where

$$C_{sc} = e\sqrt{\varepsilon_{sc} N_{Bulk}} + e^2 N_{traps} \tag{1.13}$$

The parameter N_{Bulk} is the density of bulk traps per volume and energy, whereas N_{traps} corresponds to the density of interface traps per area and energy and ϵ_{sc} is the permittivity of the semiconductor. From equation (1.13), the maximum density of interface traps can be estimated as,

$$N_{traps} = \left(SS \frac{e}{k_B T \ln 10} - 1 \right) \frac{C_i}{e^2} \tag{1.14}$$

From the transfer characteristics of the FET devices, the subthreshold swing SS is calculated from:

$$SS = \left(\frac{\partial(\log I_{ds})}{\partial V_g} \right)^{-1} \tag{1.15}$$

It is obvious from equation (1.14) and (1.15) that a low SS corresponds to a low N_{traps} which corresponds to a steeper profile of the semi-log transfer characteristics in the subthreshold region. Conversely, a high SS indicates a high N_{traps} which is reflected in a shallower profile of the semi-log transfer characteristics in the subthreshold region.

1.4.2 Research progress on PbS QD-FETs

Recently, PbS QDs have shown their potential as semiconducting active materials for FETs.[30–42] FETs are one of the main components in several advanced electronic devices such as complementary metal oxide semiconductor (CMOS)-like integrated circuits,[80–83] current regulators for displays[84–86] and themselves can be light-emitting transistors (LETs).[29,87] However, the use of PbS QDs in FETs is still challenging because they still suffer from low carrier mobility. The low carrier mobility is one of the main obstacles in understanding the charge transport within QD films and further utilizing PbS QDs for diverse applications. Therefore, improving carrier mobility in PbS QD-FETs is an important and a necessary task to understand the properties of QD films.

The origin of low carrier mobility in the devices is mostly attributed to the high number of charge carrier traps on the QD surfaces, formed during ligand exchange.[16,88] Since the charge transport in FETs takes place very close to the semiconductor/insulator interface, the interface traps on the insulator surfaces may also determine the characteristics and the performance of the devices.[89] These interface traps further reduce the carrier mobility in the devices.

Depending on the processing conditions, the stoichiometry of QDs, and ligands, PbS QD-FETs can display n-type, p-type, or ambipolar properties.[1,34] The deposition of PbS QD films is commonly performed using a layer-by-layer

(LbL) method.[31] The exchange of the long ligands into the shorter ones is done after the deposition of each oleic-acid capped film. The LbL film deposition and ligand exchange ensure complete removal of the native oleic-acid ligands. In addition, the LbL method also allows the deposition of the next PbS layer to fill the cracks on the films that are often produced after the ligand exchange process, which result in an overall shrinking of the films. Our group previously reported the increase of the carrier mobility with increasing the number of PbS layers, thus the film thickness.[31] The increase of the carrier mobility starts to saturate after reaching certain film thickness indicating that a crack-free film has been obtained.

So far, charge transport improvement in PbS QD-FETs has been obtained through the use of different capping ligands.[63] In fact, the nature of the capping ligands on the QD surfaces strongly determines the transport characteristics of the PbS QD-FETs.[69] Ambipolar properties can be obtained using short organic ligands such as 3MPA, BDT, and EDT.[31] By crosslinking PbS QDs with 3MPA, our group reported electron mobility as high as 0.03 $cm^2V^{-1}s^{-1}$.[64] Meanwhile, the hole mobility (5 x 10^{-5} $cm^2V^{-1}s^{-1}$) is much lower than the electron mobility, as has also been observed in the QD films treated with other organic ligands (EDT and BDT).[31,64] In addition, a high on-off ratio of 10^5 is achieved in devices employing SiO_2 gate dielectric.[64]

Further efforts in improving charge transport in PbS QD-FETs were done by using inorganic atomic ligands.[63] These ligands have been reported to provide a more complete passivation against carrier traps on the QD surfaces than that with organic ligands.[16,63] In addition, the films capped with inorganic ligands have shorter inter-particle distance than those capped with organic ligands, resulting in a strong increase of the film conductivity.[46,90] Despite intensive works using inorganic ligands, the mobility in the devices (with SiO_2 gate dielectric) is, however, still limited to 0.07 $cm^2V^{-1}s^{-1}$.[63] The limited charge transport is attributed to the high number of traps at the semiconductor/insulator interfaces as mentioned earlier. Passivation of the SiO_2 dangling bonds is one of important strategies that can be adopted to suppress the interface traps. To date, introducing self-assembled monolayers (SAMs) on the SiO_2 surface is one of the most effective methods to passivate the dangling bonds.[91–93] In addition, the SAMs also introduce molecular dipoles on the SiO_2 surface which affect the device properties.[91,92] However, the study of the use of SAMs in FETs has so far been limited to organic semiconductor active layers.[91–94] This opens a question if PbS QD-FETs would also benefit of the passivation of the SiO_2 surface and the introduction of molecular dipoles through the use of SAMs.

Another way to minimize the interface traps in the devices is by gating the devices with hydroxyl-free insulators. Koh et al. reported symmetric ambipolar transport in PbS QD-FETs with electron and hole mobility of 0.1 $cm^2V^{-1}s^{-1}$ using thiocyanate (SCN-) ligands employing parylene gate insulator.[33] Meanwhile,

with high-*k* dielectrics (Al_2O_3), Jo et al. reported a significant improvement in the electron mobility to 0.47 $cm^2V^{-1}s^{-1}$.[73] Further improvement of the electron mobility in PbS QD-FETs to 2 $cm^2V^{-1}s^{-1}$ was achieved by gating the devices with a new class of gate dielectric, namely ion gel.[31] The ion gel can accumulate high carrier density due to its high capacitance (1-20 $\mu F/cm^2$). The high carrier density effectively fills the traps resulting in an increase of the film conductivity and the charge carrier mobility. The above mentioned research progresses clearly show that the properties of gate insulators strongly determine the charge transport in PbS QD-FETs. As there are still many promising hydroxyl-free insulators, investigation on the use of broad types of the insulators as gate dielectrics in PbS QD-FETs still needs to be addressed. Furthermore, a comprehensive study on the electronic structures of the carrier traps in PbS QD-FETs employing different gate insulators is also important to provide understanding of the charge transport in the QD films and to potentially improve the performance of devices.

Together with the use of hydroxyl-free insulators, doping of semiconductors is one of other effective methods to improve charge transport in FETs.[95–97] Stoichiometrically, the surfaces of PbS QDs are rich in Pb, which leads to the n-type properties of the material.[34] Kagan et al reported n-type FET devices with the excess of Pb atoms on the QD surfaces.[34,35] Despite these dominant n-type properties, most literature instead reports strategies to turn them into p-type. The p-type doping of PbS QDs can be achieved by exposing the PbS films to air.[64] As mentioned earlier, the 3MPA-crosslinked devices show ambipolar properties with electron-dominated characteristics. As the devices are exposed to air, the devices display the quenching of the electron transport. Meanwhile, in the p-channel, an increase of the hole current by one order of magnitude and a significant threshold voltage shift towards positive value, indicating strong p-type doping, are displayed. The strong p-type transport of the air-exposed PbS QD-FETs is also observed in the films crosslinked with EDT ligands.[98] In line with the 3MPA-crosslinked films, the air exposure of the films with EDT ligands results in the increase of the film conductivity and hole density supporting the strong p-type doping. While the p-type doping is researched intensively mainly because of interest for the fabrication of efficient solar cells,[15,99] studies on n-type doping of PbS QDs are still limited. Koh et al reported the n-type doping of PbS QDs using cobaltocene ($CoCp_2$) molecules.[32] Although they successfully investigated the doping effect via optical absorption spectroscopy, the doped-QDs show a decrease of conductivity as measured in FETs indicating inefficient electron doping. To enable an efficient n-type doping of the semiconductors, the highest occupied molecular orbital (HOMO) level of dopant should be shallower than the conduction band (CB) of the semiconductors. Finding dopant molecules with shallow HOMO level is, however, a challenging work. Recently, benzyl viologen (BV) has been reported as promising strong n-type dopant with shallow HOMO

level.[100,101] The BV molecules have also demonstrated efficient electron doping in carbon nanotube and MoS_2 systems.[100,101] As the conduction band of PbS QDs can be tuned from shallow to deep level by using various capping ligands, doping of the QD films with BV donor molecules is also promising in improving charge transport in PbS QD-FETs.

1.5 Experimental techniques

In this section, some experimental techniques related to the electrical and optical measurements, which are used in this thesis are presented.

1.5.1 Electrical characteristic measurements

The FET electrical characteristic measurements were performed using a probe station inside an N_2-filled glovebox at room temperature. The probe station is connected to an Agilent B1500A semiconductor parameter analyzer. The I_{ds}-V_g transfer characteristics were measured by sweeping the gate voltage with some given values of source-drain voltage. Meanwhile, the I_{ds}-V_{ds} output characteristics were obtained by varying source-drain voltage with some fixed gate voltages. The detailed values of the applied source-drain voltage and gate voltage are provided in the corresponding chapters.

1.5.2 Simulation for analysis of carrier traps

In principle, the trap density of states (trap DOS) in FETs can be estimated from equation (1.14). The equation (1.14), however, can quantify the trap DOS at a certain energy level in the subthreshold regime only. Meanwhile, study on the trap DOS in a broad energy range is important to understand charge transport in the FET devices.

In this thesis, we use a computer simulation to determine the trap DOS in PbS QD-FETs. The simulation quantifies the total density of trap states, which consists of the density of bulk and interface trap states. In PbS QD-FETs, bulk traps originate from the active materials whereas the interface traps come from the gate dielectric surface. Therefore, the presence of the interface traps determines the calculated total density of trap states in the devices. The computer simulation is based on a numerical model developed by Oberhoff et al.[102] The model uses the effective medium approach where it is assumed that the material between the source and the drain electrodes is homogeneous. Therefore, the trap states in the material are assumed to be homogeneously distributed over the whole channel region. The computer simulation works by solving drift-diffusion current (J) and Poisson equation,

$$J = e\mu\left(E\rho - \frac{k_B T}{e}\frac{\partial \rho}{\partial x}\right) \quad (1.16)$$

$$\frac{\partial^2 V}{\partial x^2} = -\frac{e\rho}{\varepsilon_o \varepsilon_s} \quad (1.17)$$

where E, ρ, T, and ε_s are electric field, carrier density, temperature, and semiconductor permittivity, respectively. In the effective medium, the drift-diffusion equation is solved self-consistently under the given boundary conditions (V_{ds}, V_g, channel length L, channel width W, etc). The input parameters are all macroscopically measurable except the number of trap states in the band gap. The trap DOS is determined by fitting the simulated curves to the measured ones. As the only free input parameter is the density of states, the spectral distribution of trap states can be unambiguously determined.

For every step in the simulation, the number of total charge carriers is calculated, which directly determines the position of the Fermi level. Depending on the energy, charge carriers are separated into free charge carriers, residing in the transport level, and trapped charge carriers, energetically positioned in the band gap. The energy, which divides these two states is the mobility edge. When the gate voltage increases, the number of charge carriers is increased and therefore also the Fermi level shifts closer to the respective transport level. This changes not only the total number of charge carriers, but also the ratio of free vs. trapped charges and thus the electric current. This enables us to determine the trap DOS directly from the measured transfer curves.

1.5.3 Optical absorption spectroscopy

Optical absorption spectroscopy is a technique that characterizes the absorption of electromagnetic radiation as a function of the wavelength. In this thesis, optical absorption measurements are used to characterize the excitonic wavelength and therefore the dimension of QDs and their level of quantum confinement. When a photon is absorbed by QDs, an electron is excited to a higher energy level. As mentioned in the previous section, charge carriers in QDs can only occupy certain discrete energy levels. Therefore, QDs only absorb photons with certain wavelengths. In PbS QDs, the measured excitonic peak in the absorbance spectra corresponds to the absorbed photon energy to excite an electron from E_{h1} to E_{e1}, thus close to the band gap energy, as demonstrated in Figure 1.3.

Absorption spectroscopy is based on the Beer Lambert law. When light with initial intensity I_o irradiates a material, it is partly absorbed and partly transmitted by the material. For a solution of QDs, the number of particles determines the amount of absorbed light, which is proportional to the concentration of solution c

and the length of light's path Δx in the sample. The transmitted light intensity is written as,

$$I = I_o e^{-c\varepsilon\Delta x} \quad (1.18)$$

where ε is absorption coefficient. From equation (1.18), the absorbance, A, is defined as,

$$A = \log\left(\frac{I_o}{I}\right) \quad (1.19)$$

The optical absorption measurements were recorded by using a double beam spectrometer (Shimadzu UV-3600). The spectrometer is able to precisely measure transmittance or reflectance from the ultraviolet (UV) region to near the infrared (NIR) region. The spectrometer uses InGaAs and cooled PbS detectors which work in the NIR region. For the UV to visible region, the spectrometer uses a photomultiplier tube (PMT). As the electromagnetic sources, the spectrometer has two main lamps which operate in two spectral ranges namely a Deuterium lamp for the UV range and a Tungsten lamp for the visible and NIR regions. A single wavelength of the lamp spectrum is selected by a double-grating monochromator.

1.6 Outline of the thesis

In this thesis, the study of charge carrier transport and the analysis of the electronic structures of carrier traps in PbS QD-FETs are reported. Our focus is to understand how the properties of the semiconductor and/or insulator interfaces and the introduction of dopant molecules on the semiconductor films can determine the charge carrier transport and the electronic structures of carrier traps in field-effect transistors. In detail:

In chapter 2, the effect of various self-assembled monolayer (SAM) treatments of the SiO_2 surface on the electrical characteristics of the devices is investigated. The use of SAMs induces molecular dipoles on the SiO_2 surface which control the type of doping in the devices. The threshold voltage of the devices was found to be proportional to the SAM doping concentration, providing an opportunity to tune the properties of PbS QD-FETs toward n- or p-type depending on the type of SAM molecules used.

In chapter 3, the charge transport properties in PbS QD-FETs through the passivation of dangling bonds on the SiO_2 surface and the use of Cytop as hydroxyl-free gate dielectric are investigated. We found that the SiO_2 surface passivation using hexamethyldisilazane self-assembled monolayers (HMDS SAMs) promotes better organization of particle assembly and reduces interface traps, resulting in the improvement of charge carrier mobility. We then found that the charge carrier mobility is further improved by one order of magnitude with

Cytop gating. Finally, the calculation of the trap density of states (trap DOS) using a computer simulation method, explains that the reduced trap DOS is a microscopic origin of the improved charge carrier mobility in the devices.

In chapter 4, the trap DOS in PbS QD-FETs employing several gate insulators with a wide range of dielectric constants is investigated. The trap DOS was found to increase with increasing the gate dielectric permittivity. In addition, the broadening of the trap DOS with increasing the dielectric polarization strength was observed. The increase and the broadening of the trap DOS originate from dipolar disorder which appears at strong dielectric polarization (high gate dielectric constant). Despite the increase of the trap DOS, we demonstrate the absence of negative effect of high gate dielectric permittivity on the charge carrier mobility at the highest applied gate voltages.

In chapter 5, an efficient n-type doping of PbS QD solids using benzyl viologen (BV) donor molecules is demonstrated. The doping strategy relies on combining the use of the donor molecules with the engineering of the QD energy level through the use of appropriate capping ligands. The BV doping enabled controlling the properties of PbS QD-FETs from ambipolar to heavy n-type allowing improving the electron mobility in the devices by one order of magnitude. In addition, the doping reduced the contact resistance of the devices to 0.77 kΩcm. The 4-terminal conductivity transistor measurements confirmed the efficient doping of the devices, which display electron mobility of 0.64 $cm^2V^{-1}s^{-1}$ employing SiO_2 gate dielectric.

Finally, in chapter 6, the effect of mechanical strain on the electron transport properties in PbS QD-FETs is investigated. An ion gel which is able to accumulate high carrier concentration was used as gate dielectric, resulting in electron mobility as high as 2.1 $cm^2V^{-1}s^{-1}$. With the application of compressive strain, we observed the improvement of the electron mobility up to 45% (mobility of 3 $cm^2V^{-1}s^{-1}$) at 2% strain. The improvement of the mobility is attributed to the reduced inter-QD spacing due to the bending of crosslinking ligands. When strain was applied in the opposite direction, we observed the decrease of the electron mobility due to the increase of the distance between QDs. In addition, we found that the application of strain influences the property of the trap states in PbS QD-FETs as indicated by the modulated threshold voltages.

1.7 References

[1] D. V Talapin, J.-S. Lee, M. V Kovalenko, E. V Shevchenko, *Chem. Rev.* **2010**, *110*, 389.
[2] C. B. Murray, C. R. Kagan, M. G. Bawendi, *Science.* **1995**, *270*, 1335.
[3] P. Hawrylak, *Phys. Rev. B* **1999**, *60*, 5597.
[4] U. Banin, Y. Cao, D. Katz, O. Millo, *Nature* **1999**, *400*, 542.
[5] A. P. Alivisatos, *Science.* **1996**, *271*, 933.
[6] M. S. Kang, A. Sahu, D. J. Norris, C. D. Frisbie, *Nano Lett.* **2010**, *10*, 3727.
[7] Y. Liu, M. Gibbs, J. Puthussery, S. Gaik, R. Ihly, H. W. Hillhouse, M. Law, *Nano Lett.* **2010**, *10*, 1960.
[8] L. Sun, J. J. Choi, D. Stachnik, A. C. Bartnik, B.-R. Hyun, G. G. Malliaras, T. Hanrath, F. W. Wise, *Nat. Nanotechnol.* **2012**, *7*, 369.
[9] K. A. Abel, J. Shan, J. Boyer, F. Harris, F. C. J. M. van Veggel, *Chem. Mater.* **2008**, *20*, 3794.
[10] L. Cademartiri, J. Bertolotti, R. Sapienza, D. S. Wiersma, G. von Freymann, G. A. Ozin, *J. Phys. Chem. B* **2006**, *110*, 671.
[11] Z. Liu, Y. Sun, J. Yuan, H. Wei, X. Huang, L. Han, W. Wang, H. Wang, W. Ma, *Adv. Mater.* **2013**, *25*, 5772.
[12] M. A. Hines, G. D. Scholes, *Adv. Mater.* **2003**, *15*, 1844.
[13] K. Bian, B. T. Richards, H. Yang, W. Bassett, F. W. Wise, Z. Wang, T. Hanrath, *Phys. Chem. Chem. Phys.* **2014**, *16*, 8515.
[14] I. Moreels, G. B. De, T. D. Van, Z. Hens, *J. Opt. Soc. Am. B.* **2009**, *26*, 1243.
[15] C. M. Chuang, P. R. Brown, V. Bulović, M. G. Bawendi, *Nat. Mater.* **2014**, *13*, 796.
[16] A. H. Ip, S. M. Thon, S. Hoogland, O. Voznyy, D. Zhitomirsky, R. Debnath, L. Levina, L. R. Rollny, G. H. Carey, A. Fischer, K. W. Kemp, I. J. Kramer, Z. Ning, A. J. Labelle, K. W. Chou, A. Amassian, E. H. Sargent, *Nat. Nanotechnol.* **2012**, *7*, 577.
[17] D. J. Milliron, *Nat. Mater.* **2014**, *13*, 772.
[18] Z. Ning, O. Voznyy, J. Pan, S. Hoogland, V. Adinolfi, J. Xu, M. Li, A. R. Kirmani, J. Sun, J. Minor, K. W. Kemp, H. Dong, L. Rollny, A. Labelle, G. Carey, B. Sutherland, I. Hill, A. Amassian, H. Liu, J. Tang, O. M. Bakr, E. H. Sargent, *Nat. Mater.* **2014**, *13*, 822.
[19] A. G. Pattantyus-Abraham, I. J. Kramer, A. R. Barkhouse, X. Wang, G. Konstantatos, R. Debnath, L. Levina, I. Raabe, M. K. Nazeeruddin, M. Grätzel, E. H. Sargent, *ACS Nano* **2010**, *4*, 3374.
[20] C. Piliego, L. Protesescu, S. Z. Bisri, M. V. Kovalenko, M. A. Loi, *Energy Environ. Sci.* **2013**, *6*, 3054.
[21] K. Szendrei, W. Gomulya, M. Yarema, W. Heiss, M. A. Loi, *Appl. Phys. Lett.* **2010**, *97*, 203501.
[22] K. Szendrei, M. Speirs, W. Gomulya, D. Jarzab, M. Manca, O. V. Mikhnenko, M. Yarema, B. J. Kooi, W. Heiss, M. A. Loi, *Adv. Funct. Mater.* **2012**, *22*, 1598.
[23] W. Yoon, J. E. Boercker, M. P. Lumb, D. Placencia, E. E. Foos, J. G. Tischler, *Sci. Rep.* **2013**, *3*, 2225.
[24] D. Zhitomirsky, M. Furukawa, J. Tang, P. Stadler, S. Hoogland, O. Voznyy, H. Liu, E. H. Sargent, *Adv. Mater.* **2012**, *24*, 6181.

[25] E. H. Sargent, *Nat. Photonics* **2012**, *6*, 133.

[26] V. Sukhovatkin, S. Hinds, L. Brzozowski, E. H. Sargent, *Science* **2009**, *324*, 1542.

[27] K. Szendrei, F. Cordella, M. V. Kovalenko, M. Böberl, G. Hesser, M. Yarema, D. Jarzab, O. V. Mikhnenko, A. Gocalinska, M. Saba, F. Quochi, A. Mura, G. Bongiovanni, P. W. M. Blom, W. Heiss, M. A. Loi, *Adv. Mater.* **2009**, *21*, 683.

[28] S. Pichler, T. Rauch, R. Seyrkammer, M. Böberl, S. F. Tedde, J. Fürst, M. V. Kovalenko, U. Lemmer, O. Hayden, W. Heiss, *Appl. Phys. Lett.* **2011**, *98*, 53304.

[29] J. Schornbaum, Y. Zakharko, M. Held, S. Thiemann, F. Gannott, J. Zaumseil, *Nano Lett.* **2015**, *15*, 1822.

[30] S. Z. Bisri, E. Degoli, N. Spallanzani, G. Krishnan, B. J. Kooi, C. Ghica, M. Yarema, W. Heiss, O. Pulci, S. Ossicini, M. A. Loi, *Adv. Mater.* **2014**, *26*, 5639.

[31] S. Z. Bisri, C. Piliego, M. Yarema, W. Heiss, M. A. Loi, *Adv. Mater.* **2013**, *25*, 4309.

[32] W. Koh, A. Y. Koposov, J. T. Stewart, B. N. Pal, I. Robel, J. M. Pietryga, V. I. Klimov, *Sci. Rep.* **2013**, *3*, 2004.

[33] W. Koh, S. R. Saudari, A. T. Fafarman, C. R. Kagan, C. B. Murray, *Nano Lett.* **2011**, *11*, 4764.

[34] S. J. Oh, N. E. Berry, J.-H. Choi, E. A. Gaulding, H. Lin, T. Paik, B. T. Diroll, S. Muramoto, C. B. Murray, C. R. Kagan, *Nano Lett.* **2014**, *14*, 1559.

[35] S. J. Oh, N. E. Berry, J.-H. Choi, E. A. Gaulding, T. Paik, S.-H. Hong, C. B. Murray, C. R. Kagan, *ACS Nano* **2013**, *7*, 2413.

[36] T. P. Osedach, N. Zhao, T. L. Andrew, P. R. Brown, D. D. Wanger, D. B. Strasfeld, L. Y. Chang, M. G. Bawendi, V. Bulović, *ACS Nano* **2012**, *6*, 3121.

[37] A. G. Shulga, L. Piveteau, S. Z. Bisri, M. V. Kovalenko, M. A. Loi, *Adv. Electron. Mater.* **2016**, *2*, 1500467.

[38] M. J. Speirs, D. M. Balazs, H.-H. Fang, L.-H. Lai, L. Protesescu, M. V. Kovalenko, M. A. Loi, *J. Mater. Chem. A* **2015**, *3*, 1450.

[39] S. M. Thon, A. H. Ip, O. Voznyy, L. Levina, K. W. Kemp, G. H. Carey, S. Masala, E. H. Sargent, *ACS Nano* **2013**, *7*, 7680.

[40] M. H. Zarghami, Y. Liu, M. Gibbs, E. Gebremichael, C. Webster, M. Law, *ACS Nano* **2010**, *4*, 2475.

[41] Y. Zhang, Q. Chen, A. P. Alivisatos, M. Salmeron, *Nano Lett.* **2015**, *15*, 4657.

[42] M. Zhao, F. Yang, C. Liang, D. Wang, D. Ding, J. Lv, J. Zhang, W. Hu, C. Lu, Z. Tang, *Adv. Funct. Mater.* **2016**, *26*, 5182.

[43] B.-R. Hyun, J. J. Choi, K. L. Seyler, T. Hanrath, F. W. Wise, *ACS Nano* **2013**, *7*, 10938.

[44] M. V Kovalenko, M. I. Bodnarchuk, D. V Talapin, *J. Am. Chem. Soc.* **2010**, *132*, 15124.

[45] R. W. Meulenberg, J. R. I. Lee, A. Wolcott, J. Z. Zhang, L. J. Terminello, T. van Buuren, *ACS Nano* **2009**, *3*, 325.

[46] M. V Kovalenko, M. I. Bodnarchuk, J. Zaumseil, J.-S. Lee, D. V Talapin, *J. Am. Chem. Soc.* **2010**, *132*, 10085.

[47] M. V Kovalenko, M. Scheele, D. V Talapin, *Science* **2009**, *324*, 1417.

[48] C. Kittel, Wiley, **1996**, pp. 141–195.

[49] M. Kuno, Garland Science, **2011**, pp. 169–173.

[50] A. M. Tripathi, S. Mitra, *RSC Adv.* **2014**, 10358.

[51] L. S. Li, J. Hu, W. Yang, A. P. Alivisatos, *Nano Lett.* **2001**, *1*, 349.

[52] M. V. Artemyev, V. Sperling, U. Woggon, *J. Appl. Phys.* **1997**, *81*, 6975.
[53] L. V. Titova, T. B. Hoang, H. E. Jackson, L. M. Smith, J. M. Yarrison-Rice, J. L. Lensch, L. J. Lauhon, *Appl. Phys. Lett.* **2006**, *89*, 53119.
[54] L. George, S. Sappati, P. Ghosh, R. N. Devi, *J. Phys. Chem. C* **2015**, *119*, 3060.
[55] H. M. Schmidt, H. Weller, *Chem. Phys. Lett.* **1986**, *129*, 615.
[56] D. Schooss, A. Mews, A. Eychmüller, H. Weller, *Phys. Rev. B* **1994**, *49*, 17072.
[57] L. E. Brus, *J. Chem. Phys.* **1984**, *80*, 4403.
[58] L. Brus, *J. Phys. Chem.* **1986**, *90*, 2555.
[59] G. Konstantatos, I. Howard, A. Fischer, S. Hoogland, J. Clifford, E. Klem, L. Levina, E. H. Sargent, *Nature* **2006**, *442*, 180.
[60] J. Tang, K. W. Kemp, S. Hoogland, K. S. Jeong, H. Liu, L. Levina, M. Furukawa, X. Wang, R. Debnath, D. Cha, K. W. Chou, A. Fischer, A. Amassian, J. B. Asbury, E. H. Sargent, *Nat. Mater.* **2011**, *10*, 765.
[61] R. Chaves, D. Cavalcanti, L. Davidovich, J. Kempe, J. H. Eberly, P. Milman, N. Zagury, I. Chuang, Q. Computation, R. Laflamme, G. J. Milburn, E. Wigner, E. Waks, A. G. White, I. Applebaum, P. H. Eberhard, P. G. Kwiat, W. J. Munro, E. R. Jeffrey, G. Alber, F. De Melo, *Science.* **2009**, 1417.
[62] D. N. Dirin, S. Dreyfuss, M. I. Bodnarchuk, G. Nedelcu, P. Papagiorgis, G. Itskos, M. V Kovalenko, *J. Am. Chem. Soc.* **2014**, *136*, 6550.
[63] D. M. Balazs, D. N. Dirin, H.-H. Fang, L. Protesescu, G. H. ten Brink, B. J. Kooi, M. V. Kovalenko, M. A. Loi, *ACS Nano* **2015**, *9*, 11951.
[64] D. M. Balazs, M. I. Nugraha, S. Z. Bisri, M. Sytnyk, W. Heiss, M. A. Loi, *Appl. Phys. Lett.* **2014**, *104*, 112104.
[65] D. Kim, Y. Fu, J. Kim, K.-H. Lee, H. Kim, H. Yang, H. Chae, *Nanotechnology* **2016**, *27*, 254203.
[66] M. A. Boles, D. Ling, T. Hyeon, D. V. Talapin, *Nat. Mater.* **2016**, *15*, 141.
[67] M. J. Greaney, R. L. Brutchey, *Mater. Today* **2015**, *18*, 31.
[68] M. Q. Dai, L. Y. L. Yung, *Chem. Mater.* **2013**, *25*, 2193.
[69] P. R. Brown, D. Kim, R. R. Lunt, N. Zhao, M. G. Bawendi, J. C. Grossman, V. Bulovic, *ACS Nano* **2014**, *8*, 5863.
[70] D. Kim, D. H. Kim, J. H. Lee, J. C. Grossman, *Phys. Rev. Lett.* **2013**, *110*, 1.
[71] O. I. Micic, K. M. Jones, A. Cahill, A. J. Nozik, *J. Phys. Chem. B* **1998**, *102*, 9791.
[72] M. Drndić, M. V. Jarosz, N. Y. Morgan, M. A. Kastner, M. G. Bawendi, *J. Appl. Phys.* **2002**, *92*, 7498.
[73] C. H. Jo, J. H. Kim, J. Kim, J. Kim, M. S. Oh, M. S. Kang, M. Kim, Y. Kim, B. Ju, S. K. Park, *J. Mater. Chem. C* **2014**, *2*, 10305.
[74] K. Bian, A. K. Singh, R. G. Hennig, Z. Wang, T. Hanrath, *Nano Lett.* **2014**, *14*, 4763.
[75] J.-S. Lee, M. V Kovalenko, J. Huang, D. S. Chung, D. V Talapin, *Nat. Nanotechnol.* **2011**, *6*, 348.
[76] I. N. Hulea, S. Fratini, H. Xie, C. L. Mulder, N. N. Iossad, G. Rastelli, S. Ciuchi, A. F. Morpurgo, *Nat. Mater.* **2006**, *5*, 982.
[77] K. Willa, R. Häusermann, T. Mathis, A. Facchetti, Z. Chen, B. Batlogg, *J. Appl. Phys.* **2013**, *113*, 133707.
[78] J. Jang, W. Liu, J. S. Son, D. V Talapin, *Nano Lett.* **2014**, *14*, 653.
[79] B. Blülle, R. Häusermann, B. Batlogg, *Phys. Rev. Appl.* **2014**, *1*, 1.
[80] D. K. Kim, Y. Lai, B. T. Diroll, C. B. Murray, C. R. Kagan, *Nat. Commun.* **2012**, *3*,

1216.
[81] D. J. Gundlach, K. P. Pernstich, G. Wilckens, M. Grüter, S. Haas, B. Batlogg, *J. Appl. Phys.* **2005**, *98*, 64502.
[82] G. Lu, J. Blakesley, S. Himmelberger, P. Pingel, J. Frisch, I. Lieberwirth, I. Salzmann, M. Oehzelt, R. Di Pietro, A. Salleo, N. Koch, D. Neher, *Nat. Commun.* **2013**, *4*, 1588.
[83] D. K. Hwang, C. Fuentes-Hernandez, J. B. Kim, W. J. Potscavage, B. Kippelen, *Org. Electron.* **2011**, *12*, 1108.
[84] H. Sirringhaus, N. Tessler, R. H. Friend, *Science.* **1998**, *280*.
[85] A. J. Snell, K. D. Mackenzie, W. E. Spear, P. G. LeComber, A. J. Hughes, *Appl. Phys.* **1981**, *24*, 357.
[86] C. Wang, J. Zhang, K. Ryu, A. Badmaev, L. G. De Arco, C. Zhou, *Nano Lett.* **2009**, *9*, 4285.
[87] M. A. Loi, C. Rost-Bietsch, M. Murgia, S. Karg, W. Riess, M. Muccini, *Adv. Funct. Mater.* **2006**, *16*, 41.
[88] T. Mentzel, V. Porter, S. Geyer, K. MacLean, M. Bawendi, M. Kastner, *Phys. Rev. B* **2008**, *77*, 75316.
[89] J. E. McDermott, M. McDowell, I. G. Hill, J. Hwang, A. Kahn, S. L. Bernasek, J. Schwartz, *J. Phys. Chem. A* **2007**, *111*, 12333.
[90] D. S. Chung, J. S. Lee, J. Huang, A. Nag, S. Ithurria, D. V. Talapin, *Nano Lett.* **2012**, *12*, 1813.
[91] C. Celle, C. Suspene, J. Simonato, S. Lenfant, M. Ternisien, D. Vuillaume, *Org. Electron.* **2009**, *10*, 119.
[92] S. Kobayashi, T. Nishikawa, T. Takenobu, S. Mori, T. Shimoda, T. Mitani, H. Shimotani, N. Yoshimoto, S. Ogawa, Y. Iwasa, *Nat. Mater.* **2004**, *3*, 317.
[93] J. F. M. Hardigree, T. J. Dawidczyk, R. M. Ireland, G. L. Johns, B.-J. Jung, M. Nyman, R. Osterbacka, N. Markovic, H. E. Katz, *ACS Appl. Mater. Interfaces* **2013**, *5*, 7025.
[94] C. Celle, C. Suspène, M. Ternisien, S. Lenfant, D. Guérin, K. Smaali, K. Lmimouni, J. P. Simonato, D. Vuillaume, *Org. Electron.* **2014**, *15*, 729.
[95] B. Lee, Y. Chen, A. Cook, A. Zakhidov, V. Podzorov, *J. Appl. Phys.* **2014**, *116*, 144503.
[96] C. Y. Kao, B. Lee, L. S. Wielunski, M. Heeney, I. McCulloch, E. Garfunkel, L. C. Feldman, V. Podzorov, *Adv. Funct. Mater.* **2009**, *19*, 1906.
[97] W. J. Yu, L. Liao, S. H. Chae, Y. H. Lee, X. Duan, *Nano Lett.* **2011**, *11*, 4759.
[98] E. J. D. Klem, H. Shukla, S. Hinds, D. D. MacNeil, L. Levina, E. H. Sargent, *Appl. Phys. Lett.* **2008**, *92*, 212105.
[99] M. J. Speirs, D. N. Dirin, M. Abdu-Aguye, D. M. Balazs, M. V. Kovalenko, M. A. Loi, *Energy Environ. Sci.* **2016**, *9*, 2916.
[100] D. Kiriya, M. Tosun, P. Zhao, J. S. Kang, A. Javey, *J. Am. Chem. Soc.* **2014**, *136*, 7853.
[101] A. R. Kirmani, A. Kiani, M. M. Said, O. Voznyy, N. Wehbe, G. Walters, S. Barlow, E. H. Sargent, S. R. Marder, A. Amassian, *ACS Energy Lett.* **2016**, 922.
[102] D. Oberhoff, K. P. Pernstich, S. Member, D. J. Gundlach, B. Batlogg, *IEEE Trans. Electron. Devices* **2007**, *54*, 17.